Geophysical Journal International

Geophys. J. Int. (2010) **181,** 1261–1274 doi: 10.1111/j.1365-246X.2010.04597.x

The updip seismic/aseismic transition of the Sumatra megathrust illuminated by aftershocks of the 2004 Aceh-Andaman and 2005 Nias events

F. J. Tilmann,[1] T. J. Craig,[1] I. Grevemeyer,[2] B. Suwargadi,[3] H. Kopp[2] and E. Flueh[2]

[1] *Bullard Laboratories, University of Cambridge, Madingley Road, Cambridge CB3* 0EZ, *UK. E-mail: tilmann@esc.cam.ac.uk*
[2] *IfM Geomar, Kiel, Germany*
[3] *Geotek LIPI, Bandung, Indonesia*

Accepted 2010 March 14. Received 2010 March 12; in original form 2009 December 12

SUMMARY

Great subduction earthquakes exhibit segmentation both within the rupture of individual events and in the long term history of the margin. The 2004 December 26 Aceh-Andaman and 2005 March 28 Nias event in northern Sumatra are two of the largest earthquakes in recent years, with both co- and post-seismic displacements constrained in unprecedented detail. Using aftershock locations from a temporary seismic array in the boundary region between both events and waveform modelling of large aftershocks, we demonstrate that the vast majority of aftershocks in the study region occur on the plate interface within a narrow band (<∼20 km) seaward of the outer arc high. Comparing the seismicity distribution to the co- and post-seismic displacements, we infer that the seismic band marks the transition between the seismogenic zone and stable sliding. The location of the band and therefore the transition appears to be correlated with the ∼500 m bathymetry contour. This close correspondence is disrupted at the boundary between the two great earthquakes, where the transition to seismogenic behaviour occurs further landward by ∼25 km. To the west of Simeulue, where seafloor bathymetry throughout the forearc is deeper than 500 m, the seismic band terminates abruptly and the focus of aftershock activity is found near the trench. The seismic efficiency of afterslip varies dramatically along strike: the segment below the Banyak islands, in the gap between the two main asperities of the Nias earthquake, accommodates a much larger proportion of afterslip seismically.

Key words: Seismicity and tectonics; Subduction zone processes; Indian Ocean.

1 INTRODUCTION

Earthquakes on the megathrusts of subduction zones dominate global moment release, and present a grave danger to coastal populations from both shaking and from the tsunamis they often generate. Along-strike segmentation controls the length of megathrust ruptures, and thus also has a strong influence on their total magnitude. The amplitude of the tsunami is controlled both by the amplitude of seafloor uplift or subsidence, and whether this occurs in deep or shallow water, which in turn depends on the morphology of the forearc as well as the updip limit of the seismogenic zone. The recent great earthquakes in Sumatra provide an opportunity to investigate these topics; the quality of contemporary global seismic and geodetic networks and the availability of local geodetic data from forearc islands (rare in other subduction zones) allowed the co- and post-seismic motions and associated seismicity near the updip end of the the seismogenic zone to be determined in unprecedented detail.

The 2004 December 26 Aceh-Andaman earthquake ($M_w = 9.2$) nucleated to the north of Simeulue island and ruptured predominantly northwards (Ammon *et al.* 2005; Subarya *et al.* 2006; Menke *et al.* 2006). The rupture extended southwards towards central Simeulue, as can be seen in the aftershock distribution (Engdahl *et al.* 2007) (magenta dots in Fig. 1) and uplift pattern (Meltzner *et al.* 2006; Briggs *et al.* 2006) (magenta contour in Fig. 1b). The 2005 March 28 Nias earthquake ($M_w = 8.7$) nucleated near the Banyak islands, and ruptured bilaterally, with slip maxima below northern Nias and southern Simeulue but only minor slip below the nucleation region (Briggs *et al.* 2006; Konca *et al.* 2007). The uplift pattern for both events shows ridges of maximum uplift approximately aligned with the trench-side coastlines of Simeulue and Nias (Fig. 1b). This pattern is disrupted below the Banyak islands nucleation region, where contours are more widely spaced, corresponding to the smaller slip attained there, and the line of zero elevation change is offset landwards. A pronounced minimum, sometimes referred to as the Simeulue saddle (Briggs *et al.* 2006), is separating the uplift ridges corresponding to the 2004 and 2005 earthquakes, indicating that there is a small gap separating the two events. It is not known with certainty whether the pattern just described is representative of the long term history of the margin. However, the rupture zone for an earthquake in 1861 appears to be very

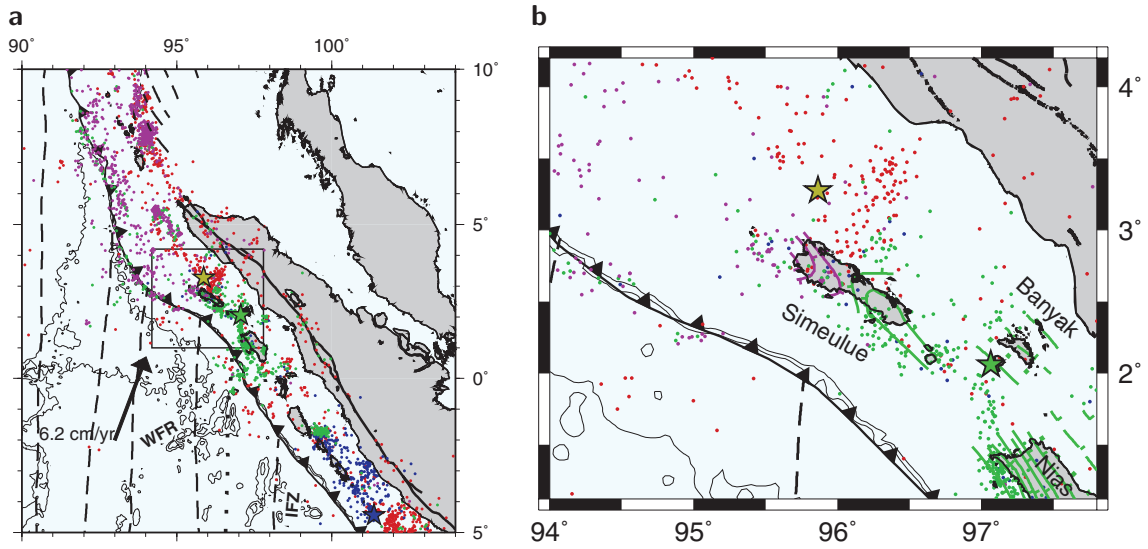

Figure 1. (a) Regional tectonics showing shallow global seismicity (magnitude>4.5, depth<50 km) from 1964 January 1 to 2004 December 25 [red, EHB (Engdahl *et al.* 2007)], between 2004 December 26 and 2005 March 27 (magenta, EHB), 2005 March 28–2006 December 31 (green, EHB) and 2007 January 1–2008 February 26 (blue, NEIC US Geological Survey 2009). Bathymetry contours at 4500 and 5000 m highlight the Investigator Fracture Zone (IFZ) and Wharton Fossil Ridge (WFR). Dashed lines show fracture zones (FZ) from Cande *et al.* (1989), and dotted line hypothesized FZ from Kopp *et al.* (2008). The rectangular box outlines the working area shown in more detail in (b) and subsequent figures. The detail view in (b) additionally shows coseismic uplift and subsidence contours from Briggs *et al.* (2006); tick marks show the direction of decreasing vertical displacement, the dotted line corresponds to zero uplift, and the dashed lines indicate subsidence; the contour interval is 0.5 m.

similar to that of the 2005 rupture, albeit with a lower estimated moment ($M_w \sim 8.4$; Newcomb & McCann 1987). Furthermore, the Simeulue saddle, that is, the boundary between the 2004 and 2005 events, coincides with a distinct kink in the Simeulue coastline, which is probably related to the change in the direction of the trench near 96°E, 2°N (e.g. Fig. 2). Similarly, at the location of the 2005 Banyak islands slip minimum, shallow water is found in the forearc instead of the basins northeast of Simeulue and Nias, and the Banyak island group consists of much smaller islands with a more complex geometry and located closer to the mainland compared to the elongated forearc islands of Simeulue and Nias. A similar disruption to the topographic pattern occurs to the south of the 2005 rupture where the Batu island group is also characterized by a complex geometry and the absence of a basin between the mainland and the islands.

Therefore, it seems at least plausible that some aspects of the rupture pattern are persistent and related to large-scale topography, where a variety of mechanisms have been proposed to explain the link (Song & Simons 2003; Wells *et al.* 2003; Wang & Hu 2006). Both Wells *et al.* (2003) and Song & Simons (2003) noticed that asperities of large megathrust earthquakes often coincide with forearc basins and lows in the trench-parallel gravity anomaly, invoking a link between subduction erosion and seismogenesis (Wells *et al.* 2003), or enhanced coupling due to an increased coefficient of friction pulling down the forearc (Song & Simons 2003). As just described, the coincidence of basins and maximum slips also occurs for the Sumatra earthquakes along strike, but not along dip, where the slip maxima appear to be focussed below the islands rather than below the basins. Finally, Wang & Hu (2006) developed the theory of the dynamic Coulomb wedge to show that the variation of the coefficient of friction through the seismic cycle can explain the low slope angles often observed above seismic aperities.

Globally located aftershocks in the study region are dominated by shallowly dipping thrust faults at depths of less then 35 km (Dewey *et al.* 2007; Engdahl *et al.* 2007). Apart from a well-defined cluster of deeper thrust events (40–50 km) between 4 and 6°N, offshore Banda Aceh and just to the north of our study region, only few teleseismically recorded aftershocks are deeper (>35 km). Unusual very shallow reverse faulting activity with somewhat variable dips and strikes is found near the trench west of 94.5°E (Dewey *et al.* 2007). French and Japanese ocean bottom seismic arrays, between 4 and 6°N, just to the north of the study region shown in Fig. 1(b), observed significant activity on forearc splays between ∼60 and 120 km from the trench (Araki *et al.* 2006; Sibuet *et al.* 2007) and in vertically oriented clusters within the downgoing plate up to a depth of ∼50 km, and probably associated with reactivated Indian ocean fracture zones (Lin *et al.* 2009). Aftershocks have been observed to preferentially occur outside the main asperities in a number of previous megathrust earthquakes (Das & Henry 2003), and this general observation also applies to the 2004 and 2005 Sumatra earthquakes (Hsu *et al.* 2006).

In the following, we will investigate the seismic/aseismic transition, which is causing this behaviour (e.g. Perfettini & Avouac 2004), and examine its variation along strike, based on seismicity data from a temporary deployment of ocean bottom seismometers and land stations in North Sumatra, waveform modelling of teleseismically recorded aftershocks within and near the region where the temporary array was deployed, and a comparison of cumulative moment release of aftershocks and geodetically determined postseismic displacement.

2 LOCAL AFTERSHOCK SURVEY

2.1 Method

Our study focuses on the southernmost part of the Aceh-Andaman rupture, and the central and northern part of the Nias earthquake, encompassing the boundary between the two earthquakes. We deployed a combined seismic array on and around Simeulue comprising 40 ocean bottom instruments (OBS and OBH, type

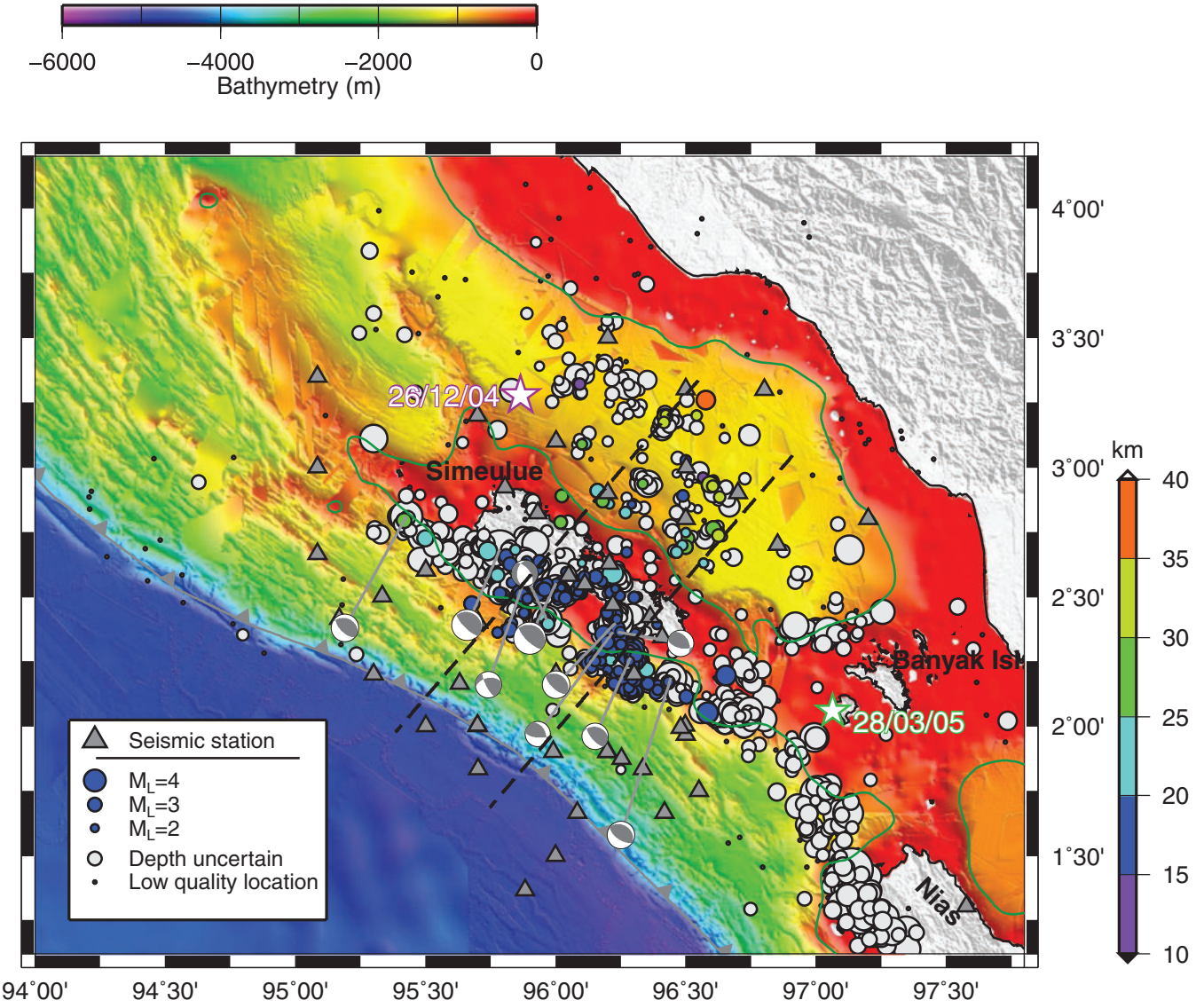

Figure 2. Local earthquake locations. Local earthquakes in the context of seafloor topography. Multibeam bathymetry is merged from data acquired on German (Kopp *et al.* 2008), French (Graindorge *et al.* 2008) and UK cruises (Henstock *et al.* 2006; Dean *et al.* 2008); SRTM30_PLUS is used for land topography, and seafloor not covered by multibeam (Becker *et al.* 2009). Where available, GCMT solutions are plotted at their global centroid location with lines connecting them to their locally determined location. Stars show the epicentres of main events (EHB), and dashed black lines show the location of the cross-sections in Fig. 6. The 500 m smoothed bathymetry contour is shown as a green continuous line.

IfM-Geomar; Bialas *et al.* 2002) and 8 land instruments (Güralp CMG-6T). This deployment was part of a major geophysical data acquisition initiative, which also involved the collection of refraction (Zillmer *et al.* 2007) and MCS profiles (Franke *et al.* 2008). The ocean bottom stations were operational between 2005 October and 2006 February, and the land stations were recording between 2005 December and 2006 March. For earthquake location we follow the approach described in more detail in Tilmann *et al.* (2008), as follows.

(i) Detect potential events based on nearly coincident STA/LTA triggers.

(ii) Manually pick arrivals and obtain a preliminary location for local and regional events (1339 events).

(iii) Using VELEST (Kissling *et al.* 1994), jointly invert for a minimum 1-D velocity model (Fig. 3) and station statics (Fig. 4), only taking into account events picked at more than 6 stations, and with an azimuthal gap less than 200°(770 events); picks with initial residuals of more than 0.75 s are considered outliers and removed from the inversion. The starting models, shown in Fig. 3(a), were generated by random perturbation, and then the inversion was iterated until convergence for each of the models. Not all of the starting models converged equally well, and we show only those final models (Fig. 3b) whose RMS is less than 10 per cent larger than the best-fit model (approximately one third of all final models). The resolution is satisfactory between 15 and 35 km, and the final models show a reasonable convergence in this depth range. Because of the paucity of shallow events, the shallow structure is not well resolved. Similarly, the deep structure varies significantly between models, with many models showing unrealistically large half-space velocities. We therefore chose among the models plotted in Fig. 3(b) the model with upper crustal velocities broadly consistent with refraction results (Zillmer *et al.* 2007) and realistic mantle velocities below 45 km, even though it had slightly

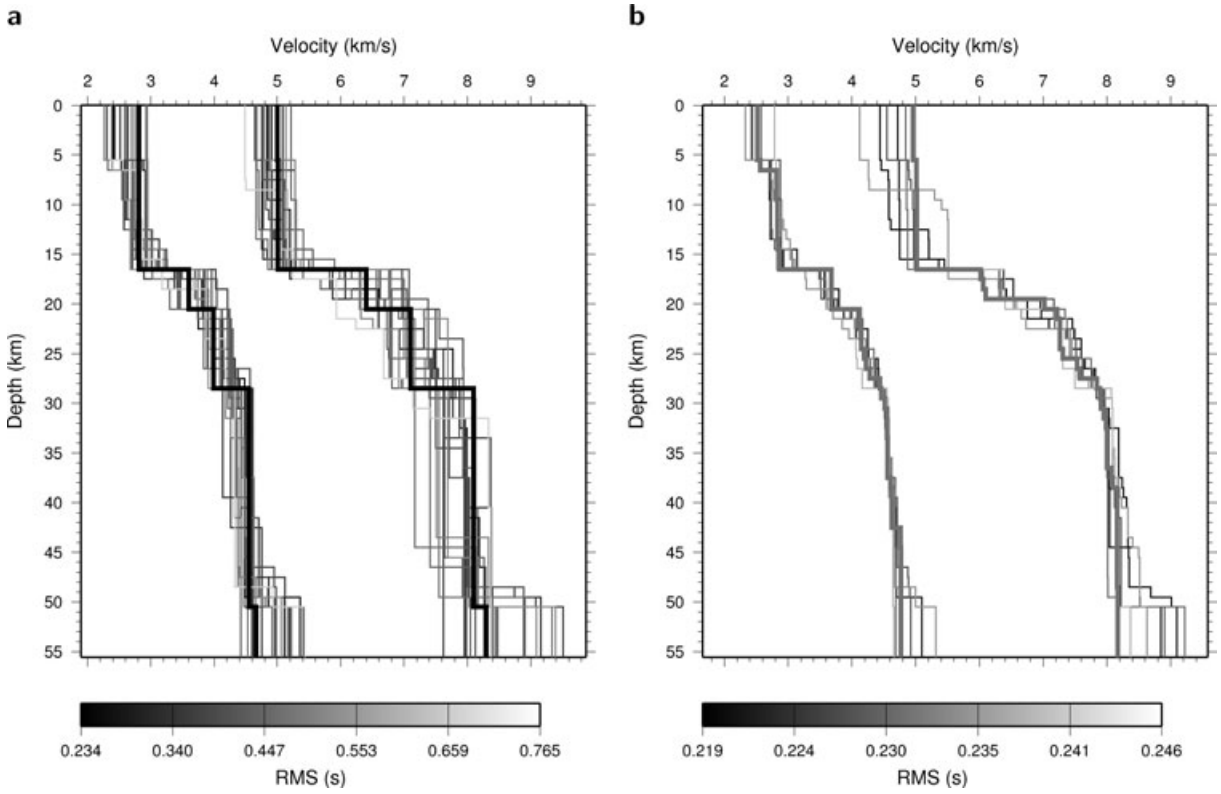

Figure 3. Starting (a) and final (b) velocity models for the 1-D inversion of events within the array. The preferred model used for all relocations is shown with a bold line in b. The colour scale indicates the rms of the models shown.

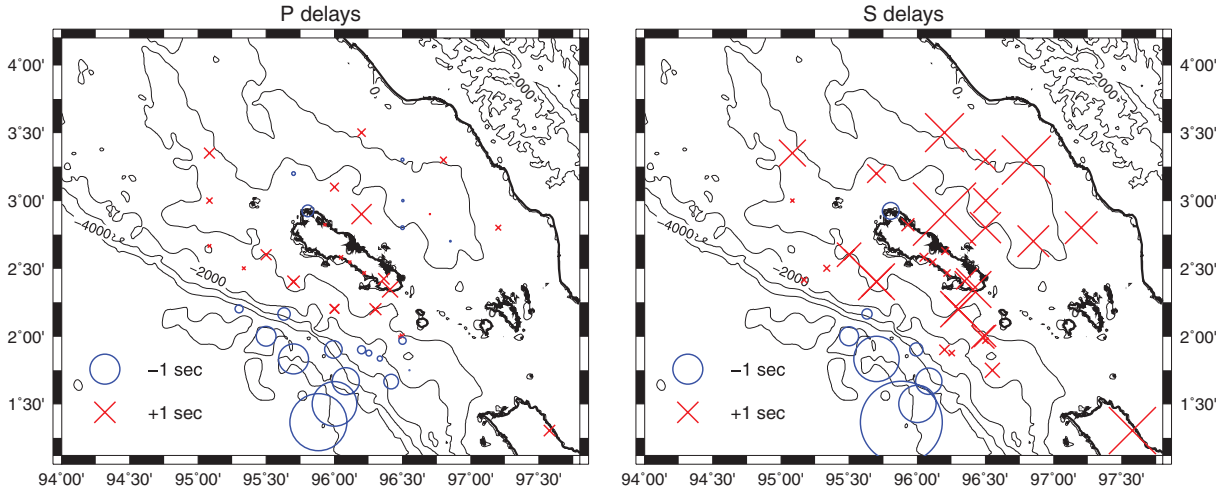

Figure 4. *P* and *S* station terms. Final *P* and *S* station statics for preferred velocity model. Note that station elevation has been taken into account explicitly, that is, the station statics represent variations of the shallow structure.

larger misfit (rms 0.231 s instead of 0.219 s) than the best-fitting model.

Generally, the station delays are similar for nearby stations and *P* and *S* delays for the same station are well correlated (Fig. 4). Stations near the trench and on the forearc slope are characterized by negative delays, presumably because of the fact that fast oceanic type crust is found relatively near the surface. Within the Simeulue basin, *S* wave delays are large compared to the *P* wave, probably reflecting high V_P/V_S ratios in the sediments.

(iv) Using the station terms and minimum 1-D velocity model relocate all events using the non-linear oct-tree search algorithm (NonLinLoc; Lomax *et al.* 2000). This method explores the probability density function, and therefore provides more reliable information on location uncertainties than linearized inversions. The maximum likelihood location is retained as the preferred location.

Events picked on at least five stations, with both *P* and *S* waves picked, an azimuthal gap of less than 300°, and a latitude and longitude error of less than 10 km are considered to have 'well-determined' epicentres (1067 events). The median horizontal error for events within this set is 3.0 km (90 per cent conf.), and the median and maximum depth errors are 3.3 and 27 km, respectively.

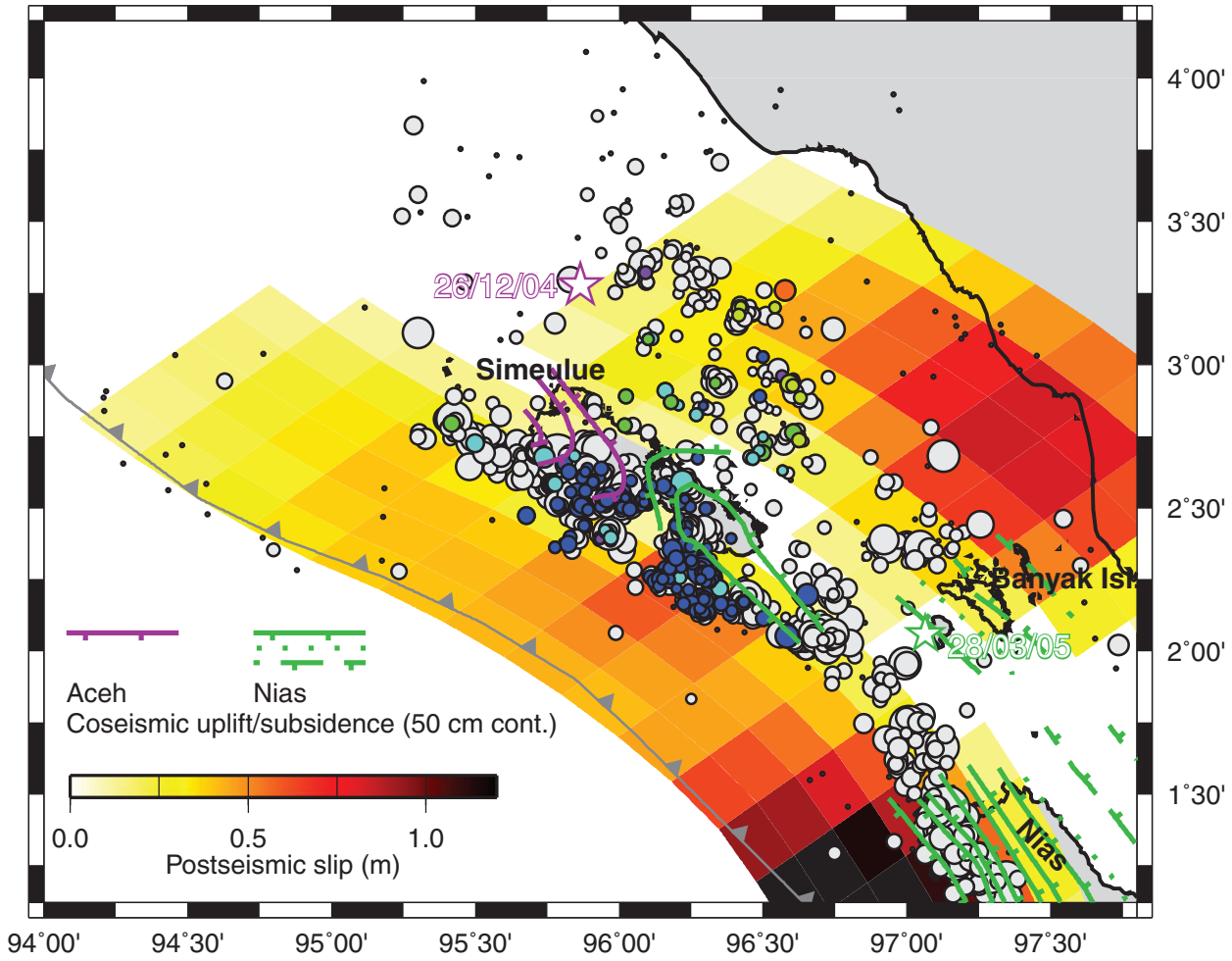

Figure 5. Earthquake locations, coseismic uplift/subsidence, and afterslip. Coseismic uplift and subsidence contours from Briggs *et al.* (2006); tick marks show the direction of decreasing vertical displacement, the dotted line corresponds to zero uplift, and the dashed lines indicate subsidence (contour interval 0.5 m). Coloured polygons show post-seismic motion between 2005 April and 2006 February estimated by Hsu *et al.* (2006). Local earthquakes are displayed using the same format as in Fig. 2.

Events with well-determined depths additionally have an azimuthal gap less than 200°, a probability of the maximum likelihood location of at least 0.05, a traveltime rms less than 0.04 s and a maximum length of 2.5 km for the longest semi-axis of the 68 per cent confidence ellipsoid. These are shown with coloured circles in Figs 2, 5 and 6 (244 events). Median and maximum horizontal errors for this set are 2.6 and 4.7 km (90 per cent conf.), respectively, and median and maximum depth errors are 1.9 and 4.3 km, respectively (see Supplementary Material for event catalogues in compact nordic format). Earthquake relocation in models with discontinuities has a tendency to result in clustering near the discontinuity. In order to test whether an apparent narrow depth range of earthquakes could be an artefact of the relocation, we also tested smooth models without discontinuities. Although these models generally showed a much poorer fit to the data, the clustering in depth for events within the seismic band still occurred for these smoothed models, that is, it cannot be an artefact of relocation in the preferred velocity model.

2.2 Results

Most of the seismicity is concentrated into a narrow 20–30 km wide band starting at 40–70 km from the trench (Fig. 2). The depth-constrained events within this band form a planar structure (Fig. 6). Even though there is some minor scatter apparent in the cross-section, the uncertainties resulting from the location procedure are such as to be consistent with the hypothesis that they all have occurred on the same plane. The onset of the band follows the 500 m bathymetry contour, irrespective of the exact distance to the trench (Fig. 2). This point also generally coincides with the plateauing of forearc profiles (Fig. 6). Activity within the band varies along strike: in the Banyak islands segment the band, though still clearly identifiable, is less well defined because of the much smaller number of events within it. West of 95°20′E, just to the west of Simeulue, activity within the band ceases abruptly. At the same point, the forearc seafloor deepens such that depths of 500 m or less are no longer encountered seaward of the forearc basin. Although this abrupt termination of the seismic band falls close to the edge of our array we are confident that it is real rather than an artefact of coverage. No cluster of poorly located events extends outward from the termination, and event sizes within the band are such that they can easily be recorded outside the array. Furthermore, the termination can also be discerned in the global data (Fig. 1), confirming that it is a general feature of the aftershock sequence. The place where the band deviates most noticeably from the strong correlation with the bathymetry is below the Simeulue saddle in central Simeulue (near 2.5°N, 96.2°E), where it curves landward such that the onset

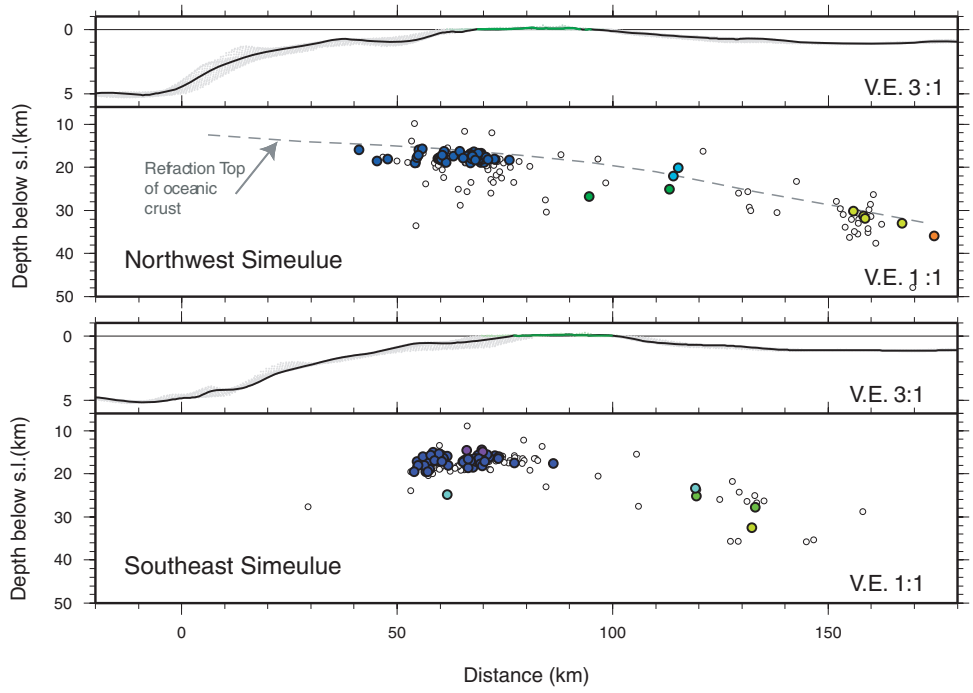

Figure 6. Trench-perpendicular cross-sections. Coloured circles are plotted for all events with well constrained depths for events within 10 km of the profile lines in Fig. 2; the colour scheme follows Fig. 2, with small white circles representing earthquakes with poor depth constraints. The bathymetry/topography along the profile lines is shown with a continuous line (in green where it is above sea level), with grey/light green shading representing the range of bathymetry/topography encountered within the swath width (10 km either side). The dotted line in the upper cross-section indicates the approximate position of the top-of-oceanic-crust interface in the refraction model of Dessa *et al.* (2009). As this profile was shot ∼90 km to the northwest of the cross-section, it had to be transposed to the section by matching the position of the trench and forearc slope. Because of this difference in locality and because the earthquakes and interface were not located with the identical velocity model their relative positions are only indicative.

of seismicity is closer to the 0 m topographic mark, some 25 km inboard of the expected location.

A smaller number of events landward of the seismic band weakly define a Benioff zone between 20 and 40 km depth, dipping at 10–15°. Based on the sparse number of events it is impossible to say whether these events occur on the plate interface or within the downgoing slab. A few events below the forearc basin are too shallow to be on or below the plate interface, and must therefore occur within the overriding plate. No events below or seaward of the islands are located reliably within the overriding plate, ruling out seismically active forearc splays as found north of 4° N (Araki *et al.* 2006; Sibuet *et al.* 2007). In fact, the whole area between the seismic band and the trench is characterized by extremely low activity, with not even a handful of events recorded along 250 km of trench in spite of OBS coverage all the way to the trench and beyond. Significant near-trench seismic activity is only found west of ∼94°75′E, well outside our array and thus mostly shown as poorly constrained in Fig. 2 but in agreement with global observations (Engdahl *et al.* 2007; Dewey *et al.* 2007 see Fig. 1) and previous OBS studies (Sibuet *et al.* 2007; Lin *et al.* 2009).

3 FOCAL MECHANISMS OF LARGE AFTERSHOCKS

3.1 Comparison with GCMT catalogue

A number of events recorded by the local array were large enough for global centroid moment tensors (GCMT) to be available (Global CMT project 2009). GCMT centroids are scattered and mostly located close to the trench but it turns out that all these events, when relocated to their locally determined location, occurred within the seismic band described above, that is, there is a significant seaward bias in the GCMT locations (Fig. 2 and Fig. S1; EHB locations tend to be biased landward, but to a lesser degree). GCMT focal mechanisms are largely consistent with slip on shallowly dipping thrust faults, but show considerable variability in their depths, dips and obliquity. Due to their reliance on long period data GCMT solutions for shallow earthquakes are susceptible to a trade-off between depth and dip angle. We therefore modelled *P* and *SH* waveforms for the largest events in the 20 months since 2005 January 1 in the Simeulue-Nias region, inverting for earthquake depth and focal mechanism.

3.2 Waveform modelling methods

Body waveform modelling techniques were applied to the 33 events with $M_w > 5.5$ occurring within the area spanning 0-4°N by 94–99°E over the 20 month period beginning 2005 January 1. Seven events failed to produce stable solutions, often due to overlap with the coda of previous events. Centroid depths and focal mechanisms were determined for the remaining 26 events. Broadband GDSN seismograms are deconvolved using a filter to reproduce the bandwidth of a 15–100 s long-period WWSSN instrument. The MT5 program of Zwick *et al.* (1994) was used to invert both *P* and *SH* arrivals within a 30–80° epicentral range, with individual waveforms being filtered for clarity of short-period arrival and signal-to-noise ratio. For events where more than 50 seismograms were available, individual waveforms were selected to retain the best possible azimuthal and epicentral coverage.

A local 1-D model is assumed in the modelling but the model is adapted for each earthquake based on actual bathymetry (Becker

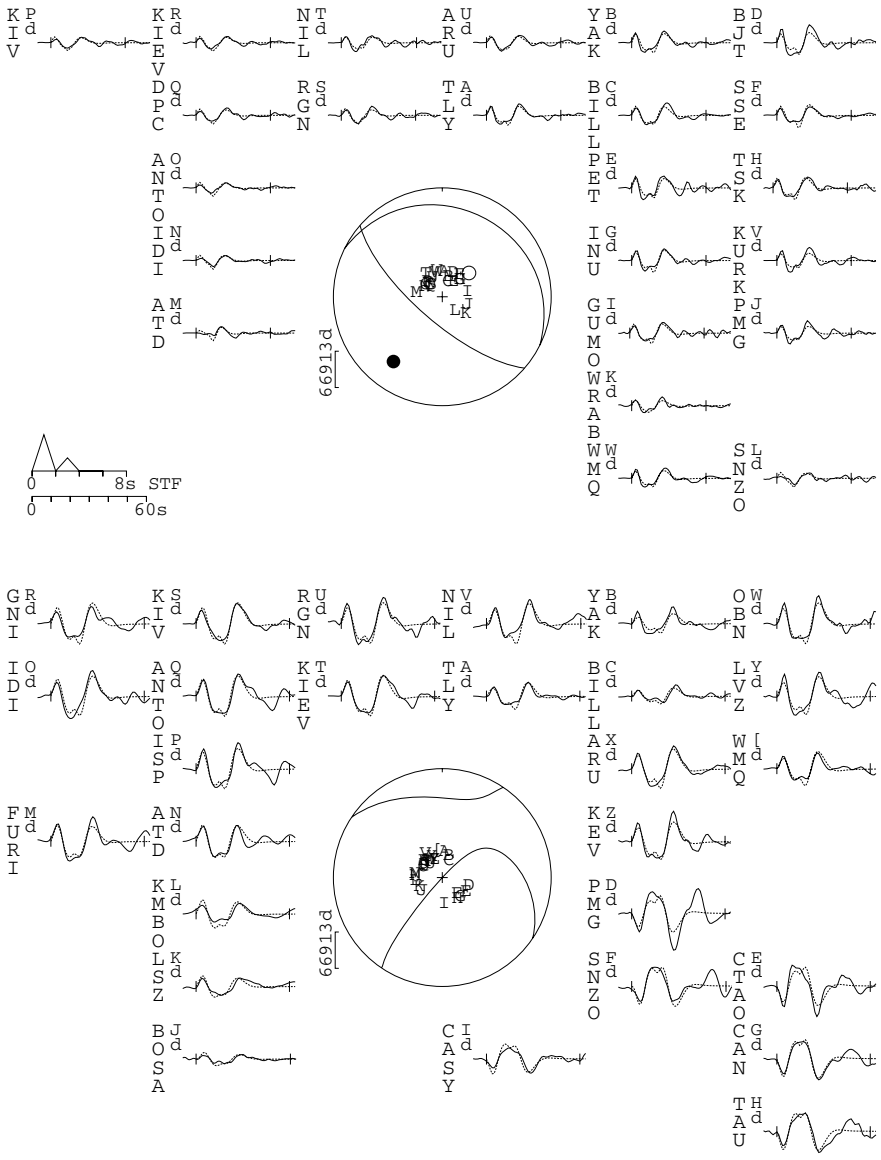

Figure 7. Event 050411 on 2005 April 11, 2.071°N, 96.683°E. Minimum Misfit Solution: Strike 296°, Dip 19°, Rake 76°, Depth 18km, M_0 8.68×10^{17}, M_W 5.9. Each individual waveform is shown at its approximate azimuth around the focal sphere appropriate to its phase (*P* at the top, *SH* at the bottom, both shown as lower hemisphere projections), designated by its station abbreviation, and letter or symbol corresponding to those shown around the focal sphere. STF represents the source-time function, with the timescale for the inverted waveforms directly below. The amplitude scale is located below and left of the *P* focal sphere, and is given in microns. Each seismogram shows the observed (solid) and synthetic (dashed) waveforms, with the window used in the inversion indicated by the vertical tickmarks.

et al. 2009), and a simplified crustal structure (water, sedimentary pile and oceanic or continental crust). This structure is determined from refraction profiles (Kopp *et al.* 2001; Zillmer *et al.* 2007) where the structure is assumed to be a function of distance from the trench along a fixed direction of N45°E, parallel to the refraction line of Zillmer *et al.* (2007). The epicentres of the events are taken from the EHB catalogue and then shifted according to the average bias between EHB and the local network (see Supplementary Material). Because the modelling code requires the source to be in the lowest layer, inversions were run with single- and two-layer crustal models, whenever events occurred close to the oceanic crust-overriding plate interface.

All events were constrained to having a purely double couple mechanism, and a source–time function comprising up to five triangular segments. Errors in depth are based on a 20 per cent relative increase in the misfit between synthetic and observed seismograms—a value typically observed to produce visible moveout of the depth phase in the synthetics. Using the event on 2005 April 11 as an example we show the waveform fit for the preferred solution in Fig. 7. This event, like most others, had a well-constrained depth, as shown by a clear minimum in the depth versus rms plot (Fig. 8); in making this plot all other parameters except depth were left to vary freely. Finally, we compare the waveform misfits of alternative solutions in Fig. 9. Equivalent plots for all events are shown in the supplementary material.

3.3 Waveform modelling results

Focal mechanisms for the 26 events that produced stable solutions are shown in Fig. 10 and listed in Table S1. Most of the events are

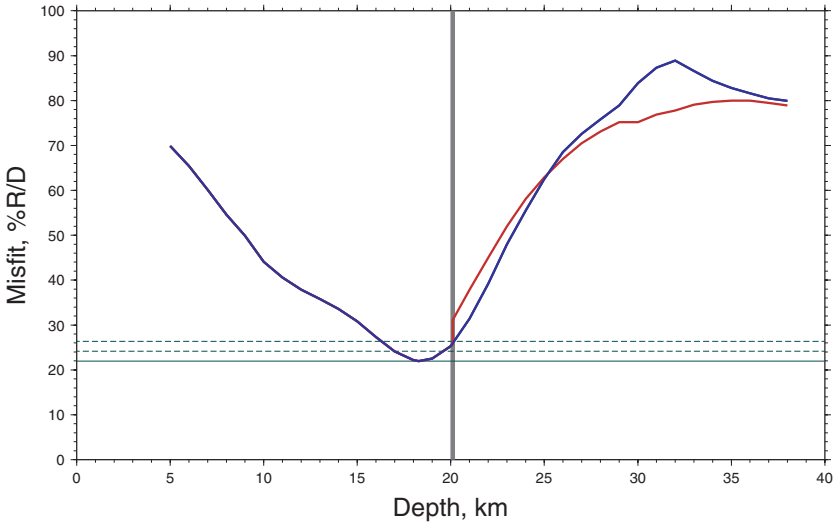

Figure 8. Depth/Misfit plot for event 050411. Minimum falls at 18.3 km depth, above the proposed crustal interface, and is constrained by a sharp step in the misfit function occurring at the crustal interface. This curve is calculated with all inversion parameters (strike, dip, rake, moment, and source time function) free, but with the depth fixed at integer kilometre values. The vertical grey line indicates the depth of the crustal interface as determined from the 2-D crustal model. The blue curve shows the misfit as calculated using a single-layer crustal model, and the red curve shows the misfit as calculated with a two layer crustal model. Horizontal grey line show the minimum misfit (solid) and the 10 and 20 per cent relative increases in misfit, used in calculating the depth errors.

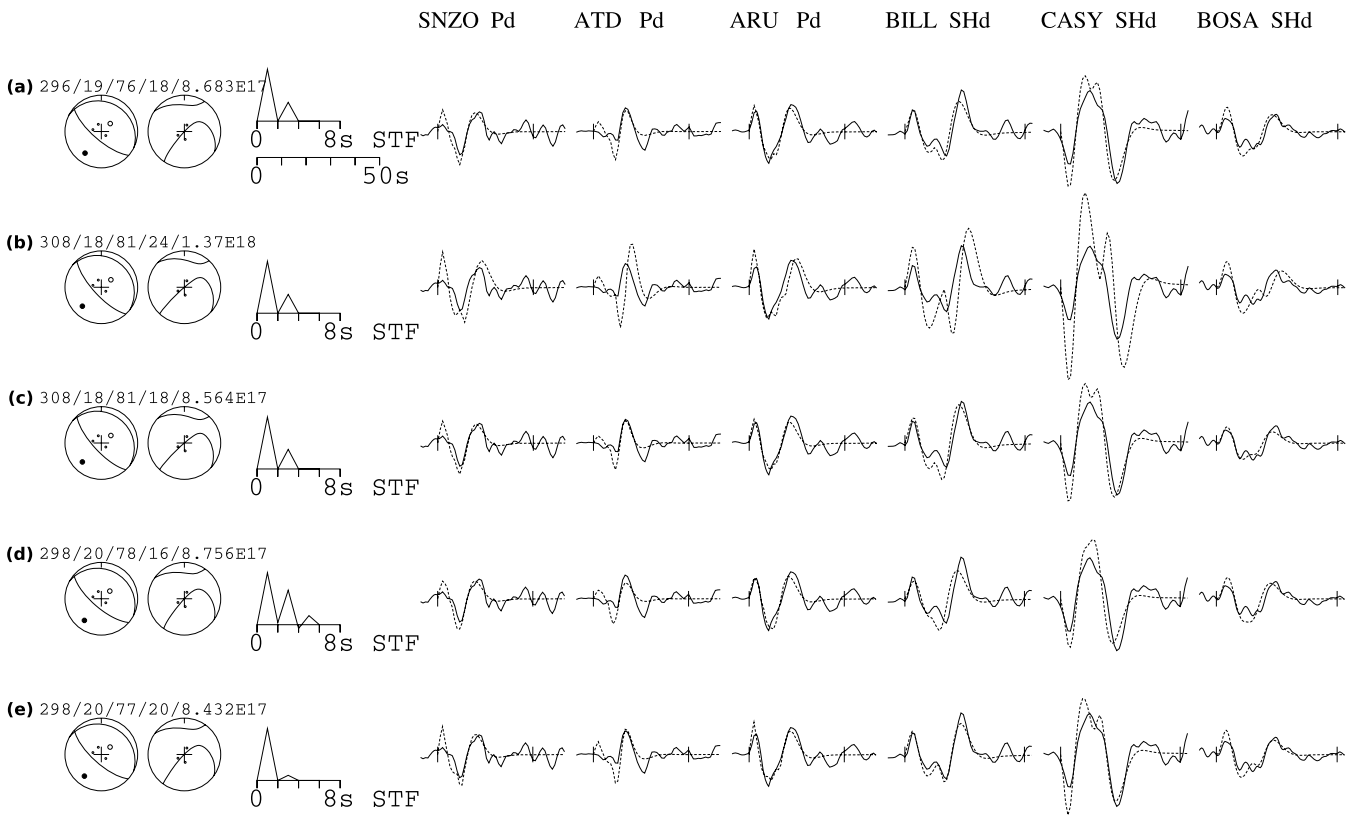

Figure 9. Error sensitivity tests for Event 050411. Six stations are plotted, chosen to have two close to the nodal planes, and one mid-quadrant, for each phase. Each line of seismograms corresponds to a different solution, with strike/dip/rake/depth/moment labelled. (a) Minimum Misfit Solution. (b) CMT Solution. Amplitude of synthetics is too great, and the depth is too great, resulting in synthetics that are too broad. The CMT depth (24 km) is the same as the EHB depth, so no seismograms are plotted using the EHB depth. (c) Inversion for depth and moment with the CMT mechanism fixed. Good fit on depth and moment, although the variation in the mechanism from the minimum misfit results in a slightly higher misfit value. (d) Depth fixed at 16.3 km. Synthetics are slightly too narrow, in particular at BILL and CASY. (e) Depth fixed at 20.2 km. Synthetics are too broad.

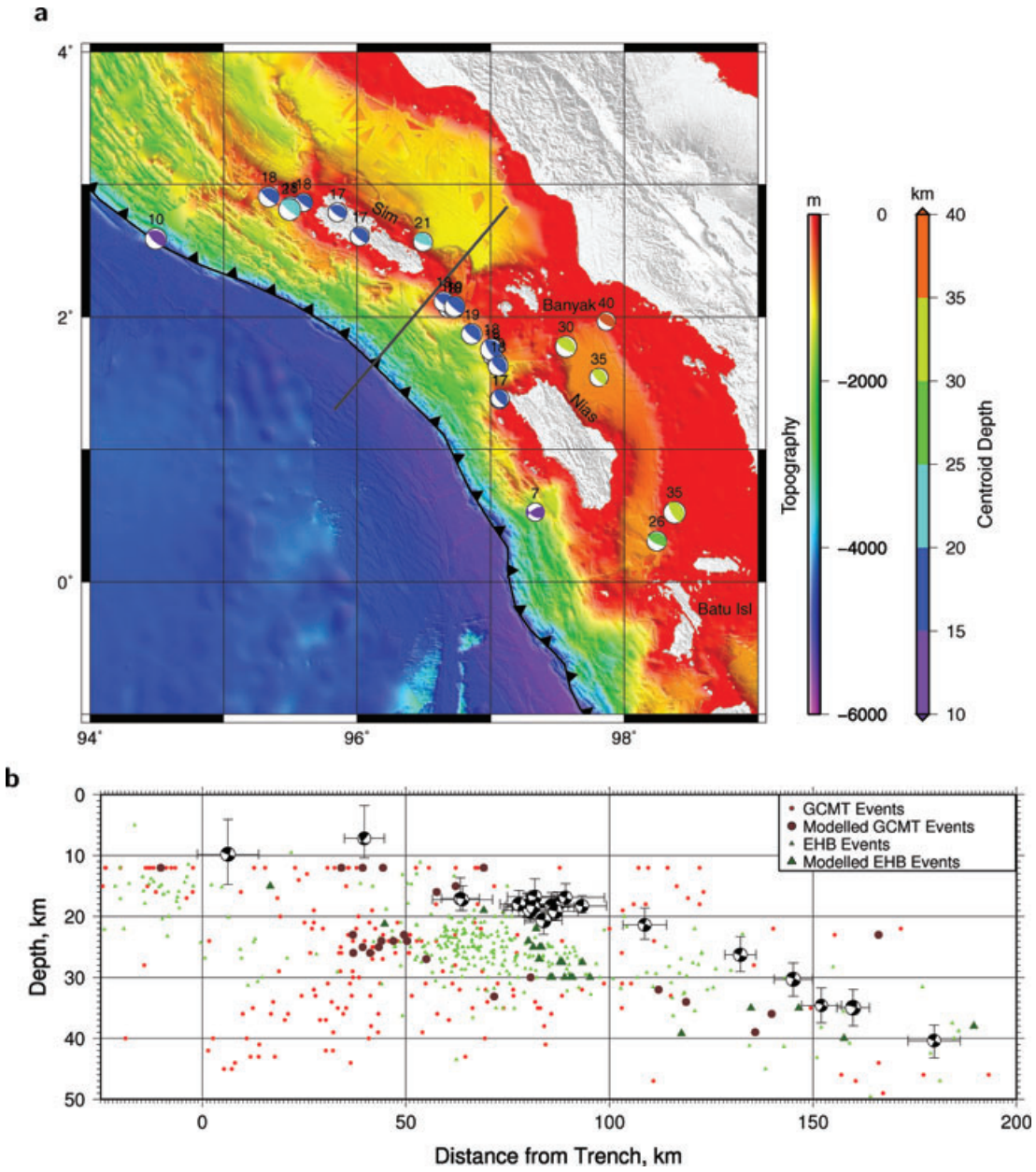

Figure 10. Waveform modelling results. (a) Focal mechanisms and depths for 26 aftershocks of the Aceh-Andaman and Nias earthquakes determined from waveform modelling of teleseismic *P* and *SH* arrivals. Numbers above focal mechanisms indicate event depth (relative to sea level). Earthquake epicentres are based on the EHB catalogue (Engdahl *et al.* 2007), corrected for bias relative to the local network locations (see Fig. S1). (b) Cross-section of modelled events projected along N40E direction. The projection is done in such a way that the 0 km distance point follows the trench axis. Waveform-modelling focal mechanism solutions are shown as hemispheres behind vertical planes; depths are derived from waveform modelling, and epicentres are EHB epicentres, corrected for bias. Large symbols show the EHB and GCMT locations of the modelled events without correction for bias. Small symbols show the EHB and GCMT locations for all events in the respective catalogues over the 20 month period studied within 0–4°N, 94–99°E (see supplementary Table S1 for a list of all event parameters). For EHB events, only those with depths reviewed and accepted during the EHB relocation process are used.

located within the seismic band at depths of 15–20 km. Although there is some scatter in the waveform-modelling derived depths, estimated uncertainties are such that all events in the seismic band could have occurred on the same plane. The scatter in depth for events in this group is less than in either GCMT or EHB catalogues (Fig. 10b), with estimated depths shallower than in the EHB catalogue by ∼5 km. The systematic shift in depth relative to EHB is probably attributable to the different velocity models used.

All events within this group are shallowly dipping thrusts. A few events landward of the seismic band and at depths greater than 20 km mark out the descending plate. Dips of these events are largely consistent with a plate interface origin (Fig. 10b). Two out of the 26 modelled events do not belong to either of these two groups. The highly oblique event to the SW of southern Nias at 7 km depth (050407 in Table S1) is placed within the overriding plate and might be associated with combined thrusting and strike-slip motion on a forearc splay, possibly in response to lower plate structures as suggested by Lin *et al.* (2009) offshore Banda Aceh. The event at 10 km depth near 2.6°N, 94.5°E (050126 in Table S1) is part of a larger group of shallow compressional

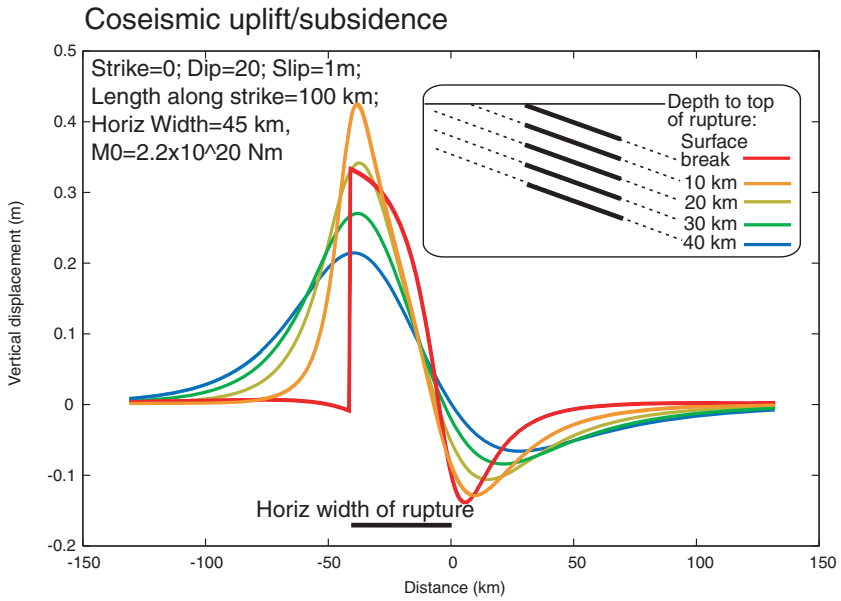

Figure 11. Predicted uplift and subsidence above a shallowly dipping thrust fault based on modelling the response of an elastic half-space to a uniform dislocation along a rectangular patch (Okada 1992). The fault parameters are listed on the top left, and curves are shown for a range of burial depths (depth to the top of the rupture). The model is not meant to represent the Sumatra megathrust in particular but to demonstrate that the uplift maximum is attained just above the updip end of the dislocation irrespective of the burial depth. Similarly, the hinge line, that is, the point of zero elevation change between uplift and subsidence is located approximately above the downdip end of the dislocation.

near-trench events (Dewey *et al.* 2007), as discussed at the end of Section 2.3.

4 DISCUSSION

4.1 Relationship of afterslip and earthquakes

The local seismicity distribution and depths and mechanisms from the teleseismic waveform modelling of aftershocks support a plate interface origin for the seismic band. The depth of the events in the band places them near the top of the oceanic crust as identified in refraction models (Zillmer *et al.* 2007; Dessa *et al.* 2009) (Fig. 6), supporting the classical model of the megathrust rupture occurring between the overriding plate and subducting oceanic crust. It is not necessary to invoke an anomalous rupture plane below the oceanic Moho as proposed recently (Singh *et al.* 2008). The absence of notable forearc seismicity below the islands argues against models invoking substantial slip on forearc splays for the 2005 earthquake (Galahaut & Catherine 2006). Elastic dislocation modelling following Okada (1992) shows that maximum coseismic uplift is achieved approximately above the updip end of the most intense coseismic rupture (Fig. 11), the position of the seismic band just seaward of the uplift ridges on Nias and Simeulue indicates that the aftershocks occur outside and just updip of the coseismic asperities. Conversely, they are found just downdip of the updip zone of significant afterslip modelled by Hsu *et al.* (2006) (Fig. 5). The events therefore appear to occur within the transition region where frictional properties along the plate interface change from aseismic behaviour/stable sliding (caused by either velocity-strengthening frictional behaviour of the fault gouge or by very low normal stresses) (Scholz 2002), to seismic behaviour/unstable sliding (requiring velocity weakening and sufficient normal stress). The updip transition in frictional behaviour is thought to occur at 100–150 °C in most subduction zones (Hyndman *et al.* 1997). Indeed, simple thermal models of the subduction zone thrust suggest that these temperatures are attained 50–70 km from the trench (Grevemeyer & Tiwari 2006), coinciding with the location of the seismic band.

Clearly, stress within the seismic band has not been released fully during coseismic rupture, presumably because too large a proportion of the plate interface is in the stable regime and thus resists rupture propagation. As a result, this region would have been highly stressed following the main rupture and thus relaxes by afterslip. On the other hand, the aftershocks within the seismic band show that the interface is not completely in the aseismic regime at this depth, and we can think of these aftershocks as essentially being driven by afterslip as proposed by Perfettini & Avouac (2004). Further updip, the plate interface is firmly in the stable regime, and afterslip is fully aseismic. A link between afterslip and aftershocks for the 2005 event was inferred previously by Hsu *et al.* (2006) based on the similar decay rates of afterslip displacements and earthquake activity. According to their estimate, only ∼7 per cent of the afterslip is released seismically. However, given the narrowness of the seismic band apparent in the local data, we can ask what proportion of afterslip within the seismic band is released seismically, that is, whether this band consists of small seismogenic patches surrounded by aseismic regions or whether deformation in this zone is still largely seismogenic, albeit prone to fail in moderate events rather than great earthquakes.

To this end, we select all aftershocks in the GCMT catalogue within the time period covered by the afterslip model (2005 March–2006 February 10) which, based on their mechanism and depth, are likely to have occurred on the plate interface (Fig. 12). We thus create a map of plate interface moment release density by distributing the moment of each selected earthquake over a radius of 25 km for the purpose of smoothing and to mitigate the location uncertainties in the global catalogue. This smoothing radius is larger than the likely rupture dimensions for any of the earthquakes within the set. The resulting plot shows a dramatic variation of the seismic moment release along strike: whereas afterslip on the updip end of the megathrust is associated with significant moment release all the

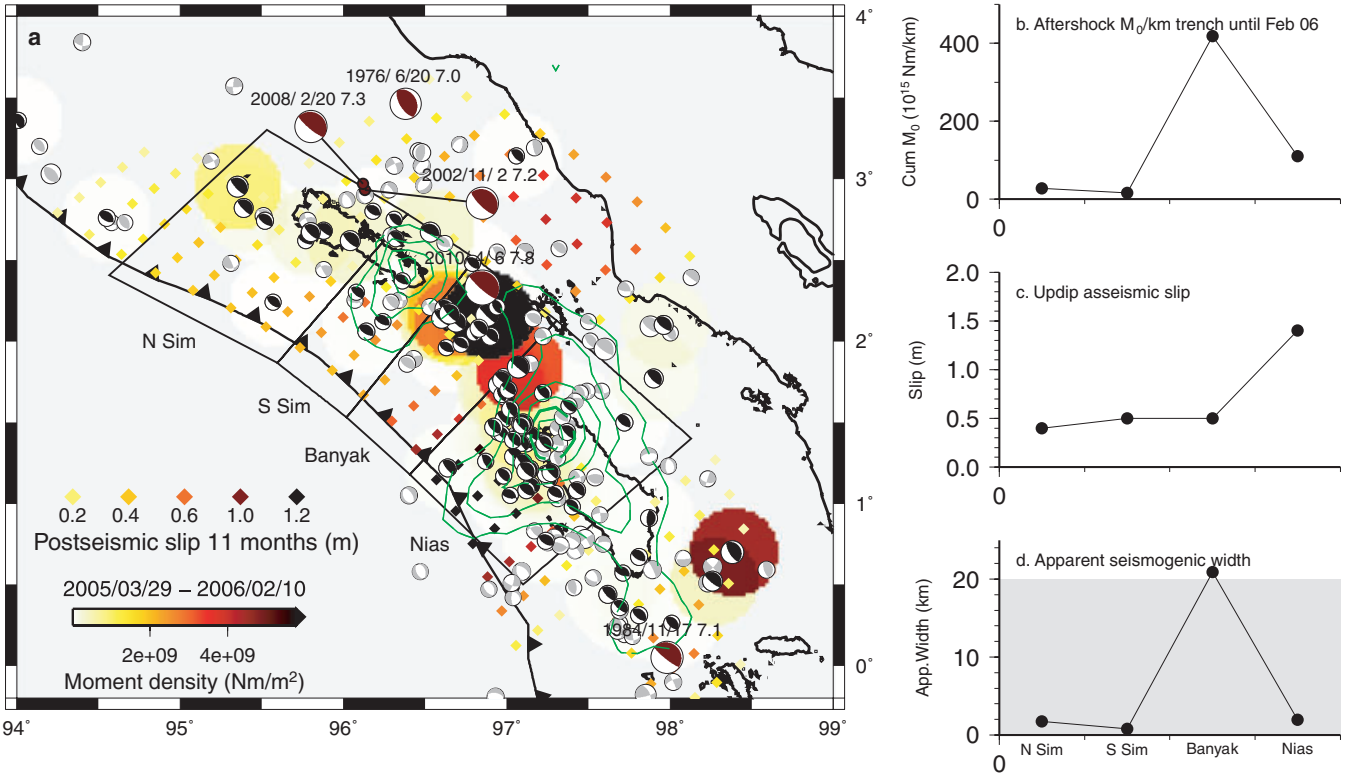

Figure 12. Moment release and afterslip. a. Focal mechanisms and cumulative moment density map of likely plate interface earthquakes for the same time period as applies to the Hsu *et al.* (2006) afterslip model (see Fig. 5; for comparison, diamonds show the afterslip model again). GCMT locations have been corrected for systematic epicentral bias. In order for an event to be classed as likely plate interface event (black focal mechanisms) it must have a GCMT solution with depth <45 km, strike 270–360°, dip 0–40° and rake 60–120°. Non-plate interface events are shown with grey focal mechanisms. Dark red focal mechanisms show events with $7.0 < M_w < 8.0$ between 1976 and 2010 with dates and magnitudes marked; the two Simeulue events have nearly identical centroids, such that their beachballs have been displaced in the plot, with a line connecting them to their actual location. The green contours show Konca *et al.*'s (2007) coseismic slip estimate for the Nias earthquake, with contours every 2 m. (b) Moment release of likely plate interface aftershocks (2005 March 29–2006 February 10) per km of trench ($\frac{M_0}{l}$) in the four regions defined in (a). (c) Cumulative afterslip u in four regions in the updip region taken from the afterslip model (Hsu *et al.* 2006) for the same time period. (d) The apparent seismogenic width w is the width over which the plate interface would need to fail seismically for the afterslip to produce the observed seismic moment release, given by $w = \frac{M_0}{l}/(\mu u)$ with shear modulus μ set to 40 GPa. The grey band indicates the approximate observed width of the aftershock seismic band.

way from west of Simeulue to at least central Nias, moment release is most intense near the Banyak islands.

Nominally, the moment release density can be converted to slip values by dividing by the shear modulus μ. However, this is misleading as the absolute values of the moment density in Fig. 12 are largely controlled by the choice of smoothing radius. Instead, we define four polygonal regions based on the segmentation of the main ruptures (Fig. 12). For each segment we compare the afterslip displacement on its updip end to the moment release per unit length of trench to calculate an apparent seismogenic width w, that is, the width of a hypothetical seismic band which would account for the observed moment release if it was fully seismogenic. The ratio of w to the observed width of the seismic band gives an indication of the proportion of the plate interface which fails seismically (within the trench distance range of the seismic band). In the Northern and Southern Simeulue and Nias segments w is less than 2 km, that is, much less than the observed width of the seismic band (Fig. 12b); moment release in Nias is larger than in Simeulue but this is balanced by larger afterslip displacements. Although uncertainties are large in the estimation of both w and the observed width of the seismic band, this result essentially confirms the view that these aftershocks arise from failure of isolated seismogenic patches driven by afterslip. Less than 10 per cent of the plate interface in these segments is seismogenic even within the seismic band, and if afterslip extends all the way to the trench (Hsu *et al.* 2006), then less than 3 per cent of the afterslip in those segments is seismogenic.

The situation is very different in the Banyak islands segment. Here, moment release is much higher in spite of afterslip displacement being comparable to the Simeulue segments, resulting in an apparent seismogenic width of ∼21 km, similar to the observed width of the seismic band. A much larger fraction of the afterslip in this region is thus associated with moment release. Moment summations are dominated by the largest earthquakes which can lead to misleading results due to sampling bias (Frohlich 2007). In order to increase our confidence in the result just stated, we also estimated moment release from the third or fifth largest earthquake, following Frohlich's (2007) suggestion. This procedure produced essentially the same result but further enhanced the differences between segments. Close inspection of the local seismicity (Fig. 2) and GCMT locations (Fig. 12a) shows that the plate interface landward of the seismic band is more active near the Banyak islands than in the other segments and has contributed significantly to the moment release; see for example the cluster of events just to the north of the Banyak islands, and at the southern edge of the Simeulue basin in Fig. 2. Even so, the seismic efficiency of afterslip is much higher below the Banyak islands than in the other segments.

Although the 2005 event nucleated in this region, coseismic slip there was moderate compared to the South Simeulue and Nias segments. Knowing this, it makes sense to find more large events on the deeper parts of the interface here as stress release was incomplete and the slip in the main asperities would have increased the Coulomb stress on the interface. The large seismic efficiency of afterslip in the Banyak segment is difficult to reconcile with proposals which explain the Banyak slip minimum in terms of predominantly aseismic conditions on the plate interface there (Hsu *et al.* 2006). Instead, stress heterogeneity might have prevented effective rupture of the Banyak segment in the great earthquake. The stress heterogeneity might be related to an hypothesized fracture zone entering the trench at ∼97°E (Kopp *et al.* 2008, also see Fig. 1). Alternatively, even though a significant proportion of the plate interface appears to be seismogenic, as just discussed, a comparatively modest areal fraction of aseismic velocity-strengthening sub-regions might be sufficient to suppress rupture propagation during the main event.

4.2 The updip transition and topography

A close correlation between seismicity and topography has been observed previously in the Chilean (Haberland *et al.* 2007; Lange *et al.* 2007) and Middle American subduction zones (Norabuena *et al.* 2004) and along the Himalayan front (Bollinger *et al.* 2004) but in most of these cases earthquakes tended to cluster at the downdip end of the locked zone. The position of the seismic band at the point where the forearc slope flattens out can be understood in terms of the theory of the dynamic Coulomb wedge (Wang & Hu 2006), where the inner wedge, which overlies the interseismically locked zone is always stable and characterized by a low surface slope. The narrowness of the seismic band attests to the abruptness of the transition between the seismogenic zone and stable sliding. The patchiness of frictional behaviour within the seismic band could then be due to small-scale variations in the normal stress, for example, due to basement topography of the incoming plate (Scholz & Small 1997) or structures within the overriding plate (Haberland *et al.* 2007). The correspondence between forearc bathymetry and updip end of the seismogenic zone, as mapped by the aftershock seismic band, thus appears to be a result of an interplay between forearc morphology and frictional properties of the plate interface, with both influencing each other and no clear cause–effect relationship being identifiable. This correspondence also raises the intriguing possibility of identifying rupture areas of future earthquakes in detail based on the bathymetry but it remains to be established how universal this feature is.

To the west of Simeulue, where the seafloor is deeper, the seismic band terminates and seismic activity is instead found near the trench. The break in forearc slope occurs in much deeper water and closer to the trench than near Simeulue, and the forearc is characterized by a series of deep basins and narrow ridges (Fig. 2). This and other morphological markers like the presence of multiple small fault scarps on landward-vergent folds on the frontal thrust might indicate that ruptures close to the prism toe are common (Henstock *et al.* 2006; McNeill *et al.* 2006) but the absence of forearc islands makes it difficult to constrain the updip extent of the 2004 coseismic rupture to the NW of Simeulue. Indications from tsunami models (Geist *et al.* 2007) and joint inversions (Chlieh *et al.* 2007; Masterlark & Hughes 2008) suggest that the rupture might have propagated to close to the trench, which would also explain the large number of near-trench events. This apparent abrupt transition in the updip extent of seismic rupture occurs in the absence of step changes in incoming plate age, convergence velocity or sediment thickness, first order parameters determining the plate interface temperatures. Because of the correspondence with forearc morphology it is likely that the 2004 and 2005 ruptures represent the full extent of the seismogenic zone. Therefore, either unusual plate interface properties cause the widely accepted transition temperature of 100–150 °C to not apply, for example, because of unusual sediment properties, or some process cools the plate prior to subduction in the Simeulue and Nias area but not in the Aceh region (W of 95°E), or there are substantial differences in the amount of sediment entrained. Further work is required to distinguish between these possibilities, but we note that the projection of the termination point of the seismic band to the trench also falls close to a change of prism morphology and frontal thrust structure along strike, with young and smooth frontal thrusts only clearly present to the NW (Henstock *et al.* 2006).

Remarkably, this dramatic transition in frictional properties is contained within the 2004 rupture, with the 2004/2005 boundary a much subtler feature and very similar seismicity patterns and forearc morphology either side of the boundary. The most notable expression of the 2004/2005 boundary is the inward curvature of the seismic band. This could simply be a reflection of the slip deficit in the gap between the 2004 and 2005 earthquakes. Alternatively, the updip end of the seismogenic zone is found further landward at this boundary. We prefer the latter explanation because the events appear to be clearly connected to the seismic band rather than forming a separate group. Two major earthquakes in 2002 and 2008, with M_w 7.2 and 7.3, respectively, occurred northeast of the Simeulue saddle, clearly downdip of the seismic band (Fig. 12) and these go some way to reduce the slip deficit left behind by the great earthquakes (DeShon *et al.* 2005), in a manner reminiscent of the plate interface seismicity near the Banyak islands discussed above but on a different timescale. It is not clear what causes this landward displacement of the onset of the seismogenic zone, but several authors have proposed a fracture zone projecting towards central Simeulue (Cande *et al.* 1989; Franke *et al.* 2008), which could be a locus of enhanced fluid release into the megathrust, enhancing fluid pressure there. The resulting reduction in effective normal stress could cause a delay in the onset of seismogenic behaviour (Moore & Saffer 2001; Scholz 2002). However, there is little direct evidence for a fracture zone, and reflection and refraction profiles instead show a broad rise of the basement (Franke *et al.* 2008). Whatever the ultimate reason, it appears that the ∼25 km landward shift of the updip end was sufficient to act as a barrier to southward propagation for the 2004 earthquake, and to northward propagation in the 1861 earthquake.

5 CONCLUSION

Most of the aftershocks of the 2005 Nias earthquake and the southernmost part of the 2004 Aceh-Andaman earthquake are concentrated into a narrow 20–30 km wide band at a depth of 15–20 km. The onset of the seismic band lies close to the 500 m bathymetry contour, also coinciding with the break in forearc slope associated with the outer arc high. Teleseismically determined focal mechanisms for events within the band indicate shallowly dipping thrusts with strikes parallel to the large scale trend of the margin, consistent with a plate interface origin of the seismic band. During the observational period, there is no indication of significant seismic activity on splay faults below Simeulue but sparse seismicity is recorded within the overriding plate below the Simeulue forearc basin.

The seismic band is located just seaward of the maximum coseismic uplift, that is, updip of the most intense coseismic displacement,

but downdip of the zone of pronounced afterslip (Hsu *et al.* 2006). Almost no seismic activity is seen between the trench and the band. Therefore, the seismic band appears to mark the transition region between stable sliding and the seismogenic zone. A comparison between afterslip displacements and cumulative moment release of plate interface aftershocks demonstrates that in the North and South Simeulue and Nias segments, less than 10 per cent of the plate interface within the narrow region defined by the seismic band is seismogenic, supporting the hypothesis of aftershocks being driven by afterslip and occurring on seismogenic patches within a largely aseismic background (Perfettini & Avouac 2004). In contrast to this behaviour, in the Banyak islands segment the ratio of aftershock moment release to afterslip is higher, such that the afterslip there contains a much larger contribution from the displacements of aftershocks. Notably, this segment does not have a forearc basin and was characterized by relatively low coseismic displacements in the 2005 rupture, even though this event nucleated there. Stress release within the seismogenic zone was thus incomplete in the main event, resulting in enhanced seismic activity in the post-seismic period within the central part of the seismogenic zone. This argues against a predominantly aseismic plate interface below the Banyak islands as an explanation for the moderate coseismic slip; instead, stress heterogeneity might have prevented the Banyak segment from rupturing effectively in the main event.

The seismic band is disrupted in two places. First, near the boundary between the 2004 and 2005 earthquakes in central Simeulue the seismic band curves sharply landward, indicating a delayed onset of unstable frictional conditions and reducing the width of the seismogenic zone. Second, to the west of Simeulue, where the forearc seafloor never shallows to less than ∼500 m, seismic activity within the seismic band ceases abruptly and aftershock activity jumps to the trench; also, the overriding plate becomes far more active (Araki *et al.* 2006; Sibuet *et al.* 2007). This dramatic transition in seismicity pattern occurs within the 2004 rupture zone, but is correlated with changes in morphology.

NOTE ADDED IN PROOF

On 2010 April 6 an $M_{\rm W} = 7.8$ earthquake occurred in the region of the Banyak islands: the CMT focal mechanism for this event has been added to Fig. 12. The event nucleated at a depth of approximately 31 km and ruptured primarily updip (US Geological Survey 2009). The moment tensor solution in conjunction with the finite-fault model (Global CMT project 2009; US Geological Survey 2009) indicates a shallowly dipping mechanism, such that the event is likely to have taken place on the plate interface. The location of the event falls between the two main slip patches of the 2005 Nias earthquake, and has therefore further reduced the slip deficit left behind by the Nias earthquake. The event falls within the Banyak segment, which had been identified above as the segment where the largest proportion of afterslip is accommodated seismically. The occurrence of this event is therefore consistent with our conjecture that rather than aseismic conditions being prevalent on the plate interface below the Banyak islands, the plate interface in this segment is largely seismogenic and capable of producing major earthquakes, but is not effectively ruptured in great earthquakes.

ACKNOWLEDGMENTS

We thank H. Harjono for facilitating the experiment, in particular with regard to permitting, captains L. Mallon, O. Meyer and their crews for excellent support on all legs of Sonne cruise SO186, ditto science crews, A. Guwanan and M. Shaw-Champion for invaluable field assistance, K. Priestley and S. Mitra for advice on waveform modelling and data preparation, L. McNeill, K. Sieh and D. Lange for helpful discussions, D. Robinson for a set of teleseismic JHD relocations, E. R. Engdahl and the ISC for the EHB catalogue and S. Dean, W. Weinrebe, F. Klingelhoefer and S. Ladage for merging/processing various bathymetry data sets. OBS were provided by IfM-Geomar, and land stations by SeisUK (loan 800). GEOFON provided data for station GSI. GMT and SEISAN were used in the data processing and preparation of figures. Financial support for the data acquisition was provided by the German Federal Ministry for Education and Research (BMBF), grant number 03G0186B. Comments from an anonymous reviewer and the associate editor Saskia Goes helped to further improve the manuscript. We also thank J. C. Sibuet and another anonymous reviewer who reviewed an earlier draft of this manuscript. Cambridge Dep. of Earth Sci. Publication 1363.

REFERENCES

Ammon, C.J. *et al.*, 2005. Rupture process of the 2004 Sumatra-Andaman Earthquake, *Science,* **308,** 1133–1139.

Araki, A., Shinohara, M., Obana, K., Yamada, T., Kaneda, Y., Kanazawa, T. & Suyehiro, K., 2006. Aftershock distribution of the 26 December 2004 Sumatra-Andaman earthquake from ocean bottom seismographic station, *Earth Planets Space,* **58,** 113–119.

Becker, J.J. *et al.*, 2009. Global bathymetry and elevation data at 30 arc seconds resolution: SRTM30_PLUS, *Mar. Geod.,* **32,** 355–371.

Bialas, J., Flueh, E.R., Phipps Morgan, J., Schleisiek, K. & Neuhaeuser, G., 2002. Ocean-bottom seismology in the third millennium, in *Science-Technology Synergy for Research in the Marine Environment: Challenges for the XXI Century*, Vol. 12: Develop. in Mar. Tech., eds Beranzoli, L., Favali, P. & Smirglio, G., Elsevier Science, B.V.

Bollinger, L., Avouac, J.P., Cattin, R. & Pandey, M.R., 2004. Stress buildup in the Himalaya, *J. geophys. Res.,* **109,** B11405.

Briggs, R.W. *et al.*, 2006. Deformation and slip along the Sunda megathrust in the great 2005 Nias-Simeulue earthquake, *Science,* **311,** 1897–1901.

Cande, S.C., LaBrecque, J.L., Larson, R.L., Pitman, W.C., Golovchenko, X., &Haxby, W.F., 1989. Magnetic lineations of the worlds ocean basins, scale: 1: 27,400,000, Am. Assoc. Pet. Geol., Tulsa.

Chlieh, M. *et al.*, 2007. Coseismic slip and afterslip of the great M_W 9.15 Sumatra-Andaman earthquake of 2004, *Bull. seism. Soc. Am.,* **97**(1A), S152–173.

Das, S. & Henry, C., 2003. Spatial relation between main earthquake slip and its aftershock distribution, *Rev. Geophys.,* **41**(3), 1013.

Dean, S., Barton, P., Djajadihardja, Y., Henstock, T., Gulick, S. & Permana, H., 2008. RV Sonne Cruise 198-1, 03 May-14 Jun 2008, 198-2, 18 Jun-01 Aug 2008, Cruise reports 31,32, National Oceanography Centre Southampton.

DeShon, H.R., Engdahl, E.R., Thurber, C.H. & Brudzinski, M., 2005. Constraining the boundary between the Sunda and Andaman subduction systems: evidence from the 2002 M_w 7.3 Northern Sumatra earthquake and aftershock relocation of the 2004 and 2005 great earthquakes, *Geophys. Res. Lett.,* **32,** L24307, doi:10.1029/2005GL024188.

Dessa, J.X., Klingelhoefer, F., Graindorge, D., André, C., Permana, H., Gutscher, M.-A., Chauhan, A., Singh, S.C. &SUMATRA-OBS Scientific Team, 2009. Megathrust earthquakes can nucleate in forearc mantle: evidence from the 2004 Sumatra event, *Geology,* **37,** 659–662.

Dewey, J.W., Choy, G., Presgrave, B., Sipkin, S., Tarr, A.C., Benz, H., Earle, P. & Wald, D., 2007. Seismicity associated with the Sumatra-Andaman islands earthquake of 26 December 2004, *Bull. seism. Soc. Am.,* **97,** S25–42.

Engdahl, E.R., Villaseñor, A., DeShon, H. & Thurber, C., 2007. Teleseismic relocation and assessment of seismicity (1918–2005) in the region of the 2004 M_w 9.0 Sumatra-Andaman and 2005 M_w 8.6 Nias Island great earthquakes, *Bull. seism. Soc. Am.,* **97**(1A), S43–S61.

Franke, D. *et al.*, 2008. The great Sumatra-Andaman earthquakes—imaging the boundary between the ruptures of the great 2004 and 2005 earthquakes, *Earth planet. Sci. Lett.,* **269,** 118–130.

Frohlich, C., 2007. Practical suggestions for assessing rates of seismic moment release, *Bull. seism. Soc. Am.,* **97**(4), 1158–1166.

Galahaut, V.K. & Catherine, J.K., 2006. Rupture characteristics of 28 March 2005 Sumatra earthquake from GPS measurements and its implications for tsunami generation, *Earth planet. Sci. Lett.,* **249,** 39–46.

Geist, E.L., Titov, V.V., Arcas, D., Pollitz, F. & Bilek, S.L., 2007. Implications of the 26 December 2004 Sumatra-Andaman earthquake on tsunami forecast and assessment mode for great subduction zone earthquakes, *Bull. seism. Soc. Am.,* **97,** S249–270.

Global CMT project, 2009. Global CMT catalog.

Graindorge, D. *et al.*, 2008. Impact of lower plate structure on upper plate deformation at the NW Sumatran convergent margin from seafloor morphology, *Earth planet. Sci. Lett.,* **275,** 201–210.

Grevemeyer, I. & Tiwari, V.M., 2006. Overriding plate controls spatial distribution of megathrust earthquakes in the Sunda-Andaman subduction zone, *Earth planet. Sci. Lett.,* **251,** 199–208.

Haberland, C., Rietbrock, A., Lange, D., Bataille, K. & Hofmann, S., 2007. Interaction between forearc and oceanic plate at the Central Chilean margin as seen in local seismic data, *Geophys. Res. Lett.,* **33,** L23302, doi:10.1029/2006GL028189.

Henstock, T.J., McNeill, L.C. & Tappin, D.R., 2006. Seafloor morphology of the Sumatran subduction zone: surface rupture during megathrust earthquakes? *Geology,* **34**(6), 485–488.

Hsu, Y.-J. *et al.*, 2006. Frictional afterslip following the 2005 Nias-Simeulue Earthquake, Sumatra, *Science,* **312,** 1921–1925.

Hyndman, R.D., Yamano, M. & Oleskevich, D.A., 1997. The seismogenic zone of subduction thrust faults, *Island Arc,* **6,** 244–260.

Kissling, E.W., Ellsworth, W.L., Eberhard-Philipps, D. & Kradolfer, U., 1994. Initial reference model in local earthquake tomography, *J. geophys. Res.,* **99,** 19,636–19,646.

Konca, A.O. *et al.*, 2007. Rupture kinematics of the 2005M_W 8.6 Nias-Simeulue earthquake from the joint inversion of seismic and geodetic data, *Bull. seism. Soc. Am.,* **97**(1A), S307–322.

Kopp, H., Flueh, E.R., Klaeschen, D., Bialas, J. & Reichert, C., 2001. Crustal structure of the central Sunda margin at the onset of oblique subduction, *Geophys. J. Int.,* **147,** 449–474.

Kopp, H. *et al.*, 2008. Lower slope morphology of the Sumatra trench system, *Basin Res.,* **20,** 519–529.

Lange, D., Rietbrock, A., Haberland, C., Bataille, K., Dahm, T., Tilmann, F.&Flüh, E.R., 2007. Seismicity and geometry of the South-Chilean subduction zone (41.5°S and 43.5 °S): implications for controlling parameters, *Geophys. Res. Lett.,* **34,** doi:10.1029/2006GL029190.

Lin, J.-Y., Le Pichon, X., Rangin, C., Sibuet, J.-C. & Maury, T., 2009. Spatial aftershock distribution of the 26 December 2004 great Sumatra-Andaman earthquake in the northern Sumatra area, *Geochem., Geophys. Geosyst.,* **10,** Q05006, doi:10.1029/2009GC002454.

Lomax, A., Virieux, A.J., Volant, P. & Berge, C., 2000. Probabilistic earthquake location in 3D and layered models: Introduction of a Metropolis-Gibbs method and comparison with linear locations, in *Advances in Seismic Event Location*, pp. 101–134, eds Thurber, C.H. & Rabinowitz, N., Kluwer, Amsterdam.

Masterlark, T. & Hughes, K.L.H., 2008. Next generation of deformation models for the 2004 M9 Sumatra-Andaman earthquake, *Geophys. Res. Lett.,* **35,** L19310, doi:10.1029/2008GL035198.

McNeill, L., Henstock, T., Tappin, D. & Curray, J., 2006. Forearc morphology and thrust vergence, sunda subduction zone (abstract), *EOS, Trans. Am. geophys. Un., Fall Meeting Supplement,* **87**(52), Abstract no. U44A-07.

Meltzner, A., Sieh, K., Abrams, M., Agnew, D.C., Hudnut, K.W., Avouac, J.-P.,&Natawidjaja, D.H., 2006. Uplift and subsidence associated with the great Aceh-Andaman earthquake of 2004, *J. geophys. Res.,* **111,** B02407, doi:10.1029/2005JB003891.

Menke, W., Abend, H., Bach, D., Newman, K. & Levin, V., 2006. Review of the source characteristics of the Great Sumatra-Andaman Islands earthquake of 2004, *Surv. Geophys.,* **27,** 603–613.

Moore, J.C. & Saffer, D., 2001. Updip limit of the seismogenic zone beneath the accretionary prism of southwest Japan: an effect of diagenetic to low-grade metamorphic processes and increasing effective stress, *Geology,* **29**(2), 183–186.

Newcomb, K.R. & McCann, W.R., 1987. Seismic history and seismotectonics of the Sunda arc, *J. geophys. Res.,* **92,** 421–439.

Norabuena, E. *et al.*, 2004. Geodetic and seismic constraints on some seismogenic zone processes in Costa Rica, *J. geophys. Res.,* **109,** B11403, doi:10.1029/2003JB002931.

Okada, Y., 1992. Internal deformation due to shear and tensile faults in a half-space, *Bull. seism. Soc. Am.,* **82**(2), 1018–1040.

Perfettini, H. & Avouac, J.P., 2004. Postseismic relaxation driven by brittle creep: a possible mechanism to reconcile geodetic measurements and the decay rate of aftershocks, application to the Chi-Chi earthquake, Taiwan, *J. geophys. Res.,* **109,** B02304, doi:10.1029/2003JB00248.

Scholz, C.H., 2002. *The Mechanics of Earthquakes and Faulting*, 2nd edn, Cambridge Univ. Press, Cambridge.

Scholz, C. & Small, C., 1997. The effect of seamount subduction on seismic coupling, *Geology,* **25,** 487–490.

Sibuet, J.-C. *et al.*, 2007. 26th December 2004 great Sumatra-Andaman earthquake: co-seismic and post-seismic motions in northern Sumatra, *Earth planet. Sci. Lett.,* **263,** 88–103.

Singh, S.C. *et al.*, 2008. Seismic evidence for broken oceanic crust in the 2004 Sumatra earthquake epicentral region, *Nat. Geosci.,* **1,** 777–781.

Song, T.R.A. & Simons, M., 2003. Large trench-parallel gravity variations predict seismogenic behavior in subduction zones, *Science,* **301,** 630–633.

Subarya, C. *et al.*, 2006. Plate-boundary deformation associated with the great Sumatra-Andaman earthquake, *Nature,* **440,** 46–51.

Tilmann, F.J., Grevemeyer, I., Flueh, E.R., Dahm, T. & Goßler, J., 2008. Seismicity in the outer rise offshore southern Chile: indication of fluid effects in crust and mantle, *Earth planet. Sci. Lett.,* **269**(1-2), 41–55.

US Geological Survey, 2009. PDE catalogue of the National Earthquake Information Center.

Wang, K. & Hu, Y., 2006. Accretionary prisms in subduction earthquake cycles: the theory of dynamic Coulomb wedge, *J. geophys. Res.,* **111,** B06410, doi:10.1029/2005JB004094.

Wells, R., Blakely, R., Sugiyama, Y., Scholl, D. & Dinterman, P., 2003. Basin-centered asperities in great subduction zone earthquakes: a link between slip, subsidence, and subduction erosion?, *J. geophys. Res.,* **108**(B10), 2507, doi:10.1029/2002JB002072.

Zillmer, M. *et al.*, 2007. First Arrival Tomography of Seismic OBS Data and Pre-stack Depth Migration of MCS Data from the Sumatra Continental Margin, *EOS, Trans. Am. geophys. Un.,* **88**(Fall Meet. Suppl.), Abstract S31C-0557.

Zwick, P., McCaffrey, R. & Abers, G., 1994. MT5 program, *IASPEI Software Library,* **4**.

SUPPORTING INFORMATION

Additional Supporting Information may be found in the online version of this article:

Table S1 and Figures S1–S79. Event bulletin in nordic format.

Please note: Wiley–Blackwell are not responsible for the content or functionality of any supporting materials supplied by the authors. Any queries (other than missing material) should be directed to the corresponding author for the article.